16th World Conference on Earthquake, 16WCEE 2017
Santiago Chile, January 9th to 13th 2017
Paper N° 1599 (Abstract ID)
Registration Code: S-R1463175909

GENERALIZED PUSHOVER ANALYSIS FOR TORSIONALLY COUPLED SYSTEMS

K. Kaatsız[(1)], F.S. Alıcı[(2)], H. Sucuoğlu[(3)]

[(1)] Research Assistant, Department of Civil Engineering, Middle East Technical University, Ankara, Turkey, kaatsiz@metu.edu.tr
[(2)] Research Assistant, Department of Civil Engineering, Middle East Technical University, Ankara, Turkey, fsalici@metu.edu.tr
[(3)] Professor, Department of Civil Engineering, Middle East Technical University, Ankara, Turkey, sucuoglu@metu.edu.tr

Abstract

Generalized pushover analysis procedure that was previously formulated on 2D planar frames is extended to 3D systems with torsional coupling in the presented study. The instantaneous force distribution acting on the system when the interstory drift at a story reaches its maximum value during seismic response is defined as the generalized force distribution. This force distribution is then expressed in terms of combinations of modal forces. Modal contributions to the generalized force vectors are calculated by a modal scaling rule which is based on the complete quadratic combination. Generalized forces are applied to the mass centers of each story incrementally for producing nonlinear static response. Maximum response quantities are then obtained when the individual frames attain their own target interstory drift values in each story. Finally, internal forces and deformations of the structural members are compiled through an envelope algorithm; registered as the inelastic seismic response of the asymmetric-plan structure.

The developed procedure is tested on a plan-asymmetric, torsionally coupled eight-story structure under a set of ground motion records which are employed without any modification. Performance of the procedure is assessed by comparing the results with those obtained from nonlinear time history analysis. Seismic response parameters such as interstory drifts and plastic rotations are presented for selected ground motions as well as mean results calculated for the ground motion set. The method is deemed successful in predicting the torsionally coupled inelastic response of 3D systems in terms of deformation and force demands.

Keywords: multi-mode pushover; torsional coupling; generalized forces; target drift; asymmetric structures

1. Introduction

Predicting the inelastic dynamic response of torsionally coupled (unbalanced) systems under strong ground excitations is perhaps one of the most challenging problems of earthquake engineering. Previous research proposed approximate methods for analysis of asymmetric-plan structures [1-2] In a comprehensive report, Rutenberg [3] concluded that the studies conducted can only be considered as a beginning in understanding the behavior of these structures. Provided that appropriate loading patterns and eccentricities are selected, he suggested pushover analysis as a promising alternative to the linear equivalent lateral force procedure. Torsionally unbalanced and irregular concrete buildings have been the subject of a study conducted by Kosmopoulos and Fardis [4]. According to the provisions of Eurocode 8 [5], they have developed a computational procedure for the analysis, evaluation and retrofitting of torsionally coupled concrete buildings. They have verified their approach by comparing the estimated demands for floor displacements and estimated member damages to the results of pseudo dynamic tests.

Pushover analysis was first applied to torsionally coupled structures by Kilar and Fajfar [6]. Later, a novel procedure where three-dimensional effects induced by higher modes and torsion were considered has been developed [7]. The implementation of multi-mode pushover analysis procedures to torsionally coupled systems is fairly recent and quite limited. Chopra and Goel [8] extended their multi-mode pushover analysis procedure MPA [9] to unsymmetrical plan buildings where the modal force vectors are composed of lateral forces and torques. After conducting modal pushover analyses with modal force vectors, seismic response of the unsymmetrical-plan structure is obtained by employing complete quadratic combination of the modal responses. Fajfar et al. [10] proposed a pushover procedure for asymmetric plan buildings which is based on the single

mode pushover analysis N2 [11]. More recently, Kreslin and Fajfar [12] combined their previous work on asymmetric buildings in both plan and elevation and extended the N2 method for these types of structures. They concluded that the proposed extended N2 method mostly yields conservative predictions of higher mode effects. Barros and Almeida [13] also suggested a new multi modal load pattern based on the relative modal participation of each mode and tested it on two story symmetrical and asymmetric structures.

Upon inspecting the past studies on torsionally coupled buildings, it can be concluded that there is still much to be developed for the seismic response prediction of these types of structures. Nonlinear time history analysis is still considered as too demanding both in computational and post processing efforts especially for analysis of simpler structures; hence there is room for simpler but reliable inelastic analysis procedures.

2. Generalized Force Vectors for Torsionally Coupled Systems

Response parameters achieve their maximum values at different time instants during seismic response. When a specific response parameter reaches its maximum value at t_{max}, there is an effective force vector acting on the system at that instant. This effective force vector includes contributions from all modes; therefore, it is a generalized force vector [14]. Upon defining the generalized force vector corresponding to a response parameter at t_{max} and applying it to the structure in a single load step, the maximum value of this response parameter can be obtained by performing an equivalent static analysis in a linear elastic system. In nonlinear systems however, generalized force vector is applied in an incremental form until a specified target response demand is attained. Interstory drift is selected as the target response parameter in this study since it provides a good representation of seismic performance of the structure at any deformation and damage state. Roof displacement is "not" employed as the control parameter in the generalized pushover procedure developed below.

Generalized force vectors are derived for linear elastic MDOF systems through the application of modal superposition principle. The maximum value of an arbitrary response parameter can be obtained at t_{max} while the system is subjected to an earthquake ground excitation $\ddot{u}_g(t)$. The force vector acting on the system at t_{max} is defined by the superposition of contributions from all modes:

$$\boldsymbol{f}(\boldsymbol{t_{max}}) = \sum_n \boldsymbol{f_n}(\boldsymbol{t_{max}}) \tag{1}$$

Effective force vector at the n'th mode is given in Eq. (2) at time t_{max}:

$$\boldsymbol{f_n}(\boldsymbol{t_{max}}) = \Gamma_n \boldsymbol{m}\boldsymbol{\varphi_n} A_n(t_{max}) \tag{2}$$

Parameters in Eq. (2) are defined below.

$$\Gamma_n = L_n / M_n \qquad L_n = \boldsymbol{\varphi_n^T m l} \qquad M_n = \boldsymbol{\varphi_n^T m \varphi_n} \tag{3}$$

Here $\boldsymbol{\varphi_n}$ is the n'th mode shape, $\boldsymbol{m}$ is the mass matrix and $\boldsymbol{l}$ is the influence vector. $A_n(t_{max})$ in Eq.(2) can be expressed in terms of the modal displacement D_n at t_{max} during seismic response:

$$A_n(t_{max}) = \omega_n^2 D_n(t_{max}) \tag{4}$$

ω_n^2 in Eq. (4) is the n'th mode vibration frequency, and D_n satisfies the equation of motion of a damped system with a modal damping ratio of ξ_n at time t_{max}.

$$\ddot{D}_n(t_{max}) + 2\xi_n \omega_n \dot{D}_n(t_{max}) + \omega_n^2 D_n(t_{max}) = -\ddot{u}_g(t_{max}) \tag{5}$$

Since $D_n(t_{max})$ occurs at a specific time during seismic excitation, it is not possible to determine it directly from Eq. (5) if t_{max} is not known. In the proposed procedure, t_{max} is defined as the time when interstory drift (Δ_j) of the j'th story reaches its maximum value.

$$\Delta_{j,max} = \Delta_j(t_{max}) \tag{6}$$

The modal expansion of $\Delta_j(t_{max})$ is given in Eq. (7):

$$\Delta_j(t_{max}) = \sum_n \Gamma_n D_n(t_{max})(\varphi_{n,j} - \varphi_{n,j-1}) \tag{7}$$

where $\varphi_{n,j}$ is the j'th element of the mode shape vector belonging to the n'th mode. Dividing both sides of Equation (7) by $\Delta_j(t_{max})$ results in the normalized form of this equation:

$$1 = \sum_n \Gamma_n \frac{D_n(t_{max})}{\Delta_j(t_{max})}(\varphi_{n,j} - \varphi_{n,j-1}) \tag{8}$$

The right hand side of Eq. (8) yields the normalized contribution of each mode n to the maximum interstory drift of the j'th story at t_{max}.

While determination of $\Delta_j(t_{max})$ still depends on t_{max}, its counterpart in Eq. (6) can be estimated through response spectrum analysis (RSA) by employing a modal combination rule. Complete quadratic combination (CQC) [15] is the best available method for combining coupled modes with closely spaced modal frequencies. $\Delta_{j,max}$ is expressed in terms of modal spectral responses obtained with RSA, combined with CQC in Eq.(9):

$$(\Delta_{j,max})^2 \approx \sum_{i=1} \sum_{n=1} \rho_{in} [\Gamma_i D_i(\varphi_{i,j} - \varphi_{i,j-1})][\Gamma_n D_n(\varphi_{n,j} - \varphi_{n,j-1})] \tag{9}$$

Here, ρ_{in} is the correlation coefficient. Indices i and n denote corresponding modes and ranges from 1 to N where N is the number of modes. D_n (or D_i) is the spectral displacement of the n'th (or i'th) mode. A normalized form of Eq. (9) can also be derived by simply dividing both sides with $(\Delta_{j,max})^2$.

$$1 = \sum_{i=1} \sum_{n=1} \rho_{in} \left(\Gamma_i \frac{D_i}{\Delta_{j,max}}(\varphi_{i,j} - \varphi_{i,j-1}) \right) \left(\Gamma_n \frac{D_n}{\Delta_{j,max}}(\varphi_{n,j} - \varphi_{n,j-1}) \right) \tag{10}$$

In Eqs. (8) and (10), the normalized contributions of individual modes to the maximum interstory drift at a specified story are defined from dynamic response history and response spectrum analyses, respectively. Under the assumption of equality stated in Eq. (6), the right-hand sides of Eqs. (8) and (10) can be equated:

$$\sum_n \Gamma_n \frac{D_n(t_{max})}{\Delta_i(t_{max})}(\varphi_{n,j} - \varphi_{n,j-1}) = \sum_{i=1} \sum_{n=1} \rho_{in} \left(\Gamma_i \frac{D_i}{\Delta_{i,max}}(\varphi_{i,j} - \varphi_{i,j-1}) \right) \left(\Gamma_n \frac{D_n}{\Delta_{i,max}}(\varphi_{n,j} - \varphi_{n,j-1}) \right) \tag{11}$$

Re-introducing Eq. (6) for the denominator terms of modal responses on both sides, and leaving out similar terms in Eq. (11) results in a simplified form:

$$D_n(t_{max}) = \sum_{i=1} \rho_{ni} \frac{D_n}{\Delta_{j,max}} [\Gamma_i D_i(\varphi_{i,j} - \varphi_{i,j-1})] \tag{12}$$

The terms in brackets in Eq. (12) is $\Delta_{j,i}$, or the i'th mode contribution to the maximum interstory drift at the j'th story determined from RSA. Inserting $\Delta_{j,i}$ for the bracket term in Eq. (12) yields a further simplified expression for $D_n(t_{max})$:

$$D_n(t_{max}) = D_n \left(\frac{\sum_{i=1} \rho_{in} \Delta_{j,i}}{\Delta_{j,max}} \right) \tag{13}$$

Eq. (13) describes $D_n(t_{max})$ independent of t_{max} through RSA, accompanied with CQC. This equality is designated as the modal scaling rule, since modal displacement amplitude of the n'th mode at t_{max} is obtained by the multiplication of spectral displacement of this mode by a scale factor. The modal scaling factor is defined as the ratio of modal contribution to any response parameter to the maximum of this response parameter calculated at the j'th story. Interstory drift in the equation is the response parameter selected for this derivation.

$A_n(t_{max})$ can also be determined from Eq. (13) by multiplying both sides with ω_n^2:

$$A_n(t_{max}) = A_n \left(\frac{\sum_{i=1} \rho_{in} \Delta_{j,i}}{\Delta_{j,max}} \right) \tag{14}$$

A_n is the pseudo-spectral acceleration of the n'th mode and obtained from $A_n = \omega_n^2 D_n$, similar to Eq. (4). $f_n\ (t_{max})$ can be rewritten via Equation (14) in a form that is independent of time. Substituting $A_n\ (t_{max})$ from Eq. (14) into Eq. (1) yields:

$$\boldsymbol{f}(t_{max}) = \sum_n \left(\Gamma_n\ \boldsymbol{m}\ \boldsymbol{\varphi_n}\ A_n \frac{\sum_{i=1} \rho_{in}\ \Delta_{j,i}}{\Delta_{j,max}} \right) \tag{15}$$

As previously stated, formulation presented herein is based on interstory drift at the j'th story. Consequently, $\boldsymbol{f}(t_{max})$ in Eq. (15) is the generalized force vector that acts on the system when the j'th story interstory drift reaches its maximum value. Therefore, $\boldsymbol{f}(t_{max})$ will be denoted as $\boldsymbol{f}_j$ in the remaining part of the formulation.

Summation for all modes in Eq. (15) over all terms in the parentheses and regrouping leads to a final form of the generalized force vector:

$$\boldsymbol{f_j} = \sum_n \left(\Gamma_n\ \boldsymbol{m}\ \boldsymbol{\varphi_n}\ A_n \right) \left[\frac{\Delta_{j,n}}{\Delta_{j,max}} + \sum_{\substack{i=1 \\ i \neq n}}^{N} \left(\rho_{in} \frac{\Delta_{j,i}}{\Delta_{j,max}} \right) \right] \tag{16}$$

The generalized force vector that maximizes the j'th story interstory drift is presented in Eq. (16). This is, in fact, the force vector which is applied on the structure in an incremental form until the target interstory drift demand at the j'th story is obtained.

3. Target Interstory Drift Demand for Torsionally Coupled Systems

Maximum interstory drift demand $\Delta_j\ (t_{max})$ during ground motion excitation was defined as a function of $D_n\ (t_{max})$ in Equation (7). $\Delta_j\ (t_{max})$ can also be expressed with the implementation of modal scaling rule by substituting $D_n\ (t_{max})$ from Eq. (13) into Eq. (7):

$$\Delta_j(t_{max}) = \sum_n \Gamma_n (\varphi_{n,j} - \varphi_{n,j-1}) D_n \left(\frac{\sum_{i=1} \rho_{in}\ \Delta_{j,i}}{\Delta_{j,max}} \right) \tag{17}$$

As discussed previously, Eq. (17) expresses target drift at the j'th story of a linear elastic system which reaches its maximum value when the corresponding generalized force vector $\boldsymbol{f}_j$ is acting on the system. The effect of nonlinearity on D_n can be considered however, which is explained in the second step of the generalized pushover (GPA) algorithm given in the following section.

Generalized force vectors and their accompanying target interstory drift demands are determined by using the eigenvectors defined at the diaphragm centers of mass of a 3D structural system. In a 2D frame, all structural members are in the same frame including the center of mass, resulting in consistent deformations and member forces at the target interstory demand. Similar to the behavior of 2D frames, response of 3D plan-symmetric structures also shows no variation within a story since torsional effects are not present. Consequently, deformations and forces of all structural members in a story can be estimated accurately by employing a single demand control mechanism, namely using one target interstory demand for each story. However, this is not the case for 3D buildings where some forms of torsional rotation components exist.

It is known from structural dynamics theory that due to strong coupling of modes and torsional effects in unsymmetrical-plan buildings, maximum values of deformations and forces at different frames within a story occur at different instants, i.e., at different t_{max} values during dynamic response. The n'th mode interstory drifts of Frame k in Fig. 1 in the direction of ground excitation is related to the center mass displacements via the distance of frame to the center of mass, x_k along with both translational and rotational components of eigenvectors at the j'th story. Considering this relation, Eq. (7) is rewritten as:

$$\Delta_j^k(t_{max}) = \sum_n \Gamma_n D_n^k(t_{max}) \left[\left(\varphi_{ny,j} - \varphi_{ny,j-1} \right) + x_k \left(\varphi_{n\theta,j} - \varphi_{n\theta,j-1} \right) \right] \tag{18}$$

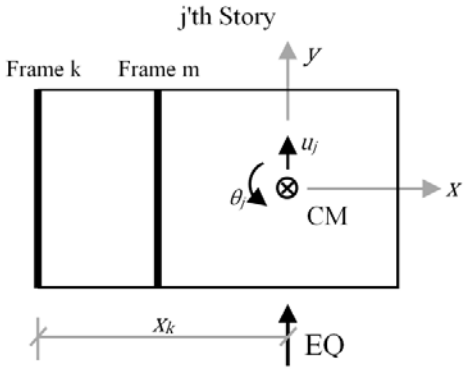

Fig. 1 – Location of Frame k with respect to the center of mass

$\Delta_j^k(t_{max})$ is the maximum value of the j'th interstory drift of Frame k and $D_n^k(t_{max})$ is the modal displacement amplitude which satisfies Eq. (5) at time t_{max}, when Δ_j^k reaches its maximum value. Normalized form of this equation with respect to $\Delta_j^k(t_{max})$ is given in Eq. (19):

$$1 = \sum_n \Gamma_n \frac{D_n^k(t_{max})}{\Delta_j^k(t_{max})}\left[\left(\varphi_{ny,j} - \varphi_{ny,j-1}\right) + x_k\left(\varphi_{n\theta,j} - \varphi_{n\theta,j-1}\right)\right] \tag{19}$$

Similarly, the combined modal response, $\Delta_{j,max}$ which is obtained from RSA through CQC is defined for Frame k in Fig. 1:

$$(\Delta_{j,max}^k)^2 = \sum_{i=1}\sum_{n=1}\rho_{in}\left[\Gamma_i D_i\left((\varphi_{iy,j} - \varphi_{iy,j-1}) + x_k(\varphi_{i\theta,j} - \varphi_{i\theta,j-1})\right)\right]\left[\Gamma_n D_n\left((\varphi_{ny,j} - \varphi_{ny,j-1}) + x_k(\varphi_{n\theta,j} - \varphi_{n\theta,j-1})\right)\right] \tag{20}$$

Eq. (20) can also be normalized with respect to $(\Delta_{j,max})^2$:

$$1 = \sum_{i=1}\sum_{n=1}\rho_{in}\left[\Gamma_i \frac{D_i}{(\Delta_{j,max}^k)}\left((\varphi_{iy,j} - \varphi_{iy,j-1}) + x_k(\varphi_{i\theta,j} - \varphi_{i\theta,j-1})\right)\right]\left[\Gamma_n \frac{D_n}{(\Delta_{j,max}^k)}\left((\varphi_{ny,j} - \varphi_{ny,j-1}) + x_k(\varphi_{n\theta,j} - \varphi_{n\theta,j-1})\right)\right] \tag{21}$$

The relation defined in Eq. (6) holds true as in the case of 2D formulation. Taking this into account, right-hand sides of Eqs. (19) and (21) can be equated:

$$\sum_n \Gamma_n \frac{D_n^k(t_{max})}{\Delta_j^k(t_{max})}\left[\left(\varphi_{ny,j} - \varphi_{ny,j-1}\right) + x_k\left(\varphi_{n\theta,j} - \varphi_{n\theta,j-1}\right)\right] = \sum_{i=1}\sum_{n=1}\rho_{in}\left[\Gamma_i \frac{D_i}{(\Delta_{j,max}^k)}\left((\varphi_{iy,j} - \varphi_{iy,j-1}) + x_k(\varphi_{i\theta,j} - \varphi_{i\theta,j-1})\right)\right]\left[\Gamma_n \frac{D_n}{(\Delta_{j,max}^k)}\left((\varphi_{ny,j} - \varphi_{ny,j-1}) + x_k(\varphi_{n\theta,j} - \varphi_{n\theta,j-1})\right)\right] \tag{22}$$

Normalized form of Eq. (20) with respect to $(\Delta_{j,max}{}^k)^2$ is inserted into the right hand side of Eq. (22) where left hand side represents the normalized form of $\Delta_j^k(t_{max})$ in terms of modal contributions. Leaving out similar terms yields $D_n^k(t_{max})$ derived for Frame k:

$$D_n^k(t_{max}) = \sum_{i=1}\rho_{in}\frac{D_n}{\Delta_{j,max}^k}\left[\Gamma_i D_i\left((\varphi_{iy,j} - \varphi_{iy,j-1}) + x_k(\varphi_{i\theta,j} - \varphi_{i\theta,j-1})\right)\right] \tag{23}$$

The term in brackets on the right hand side is the i'th mode contribution to the j'th story interstory drift of Frame k, i.e. $\Delta_{j,i}^k$. Then,

$$D_n^k(t_{max}) = D_n\left(\frac{\sum_{i=1}\rho_{in}\Delta_{j,i}^k}{\Delta_{j,max}^k}\right) \tag{24}$$

The modal expansion of the j'th interstory drift occurring at t_{max} in Frame k, i.e. $\Delta_j^k(t_{max})$ was already defined in Eq. (18). If $D_n^k(t_{max})$ is substituted from Eq. (24) into Eq. (18), then $\Delta_j^k(t_{max})$ can be expressed in terms of modal spectral responses by employing the modal scaling rule:

$$\Delta_j^k(t_{max}) = \sum_n \Gamma_n \left[\left(\varphi_{ny,j} - \varphi_{ny,j-1} \right) + x_k \left(\varphi_{n\theta,j} - \varphi_{n\theta,j-1} \right) \right] D_n \left(\frac{\sum_{i=1} \rho_{in} \Delta_{j,i}^k}{\Delta_{j,max}^k} \right) \tag{25}$$

This is in fact the target interstory drift value of Frame k in the j'th story. Similar to 2D formulation, it can be labeled as Δ_{jt}^k and expressed in open form in Eq. (26):

$$\Delta_{jt}^k = \sum_n \Gamma_n D_n \left[\left(\varphi_{ny,j} - \varphi_{ny,j-1} \right) + x_k \left(\varphi_{n\theta,j} - \varphi_{n\theta,j-1} \right) \right] \left[\frac{\Delta_{j,n}^k}{\Delta_{j,max}^k} + \sum_{\substack{i=1 \\ i \neq n}}^{N} \left(\rho_{in} \frac{\Delta_{j,i}^k}{\Delta_{j,max}^k} \right) \right] \tag{26}$$

The formulation given above is valid for two-way asymmetry, however the target interstory drift in Eq. (26) is defined for the frames oriented in the y direction. When the subscripts y are replaced by x in modal vectors and the moment arm x_k is replaced by y_k, Eq. (26) becomes valid for the x direction frames as well.

Eq. (26) yields the target interstory drift demand of Frame k at the j'th story under ground motion excitation. A similar force vector $\boldsymbol{f}_j^k$ can also be defined for Frame k by following the same procedure above. Therefore, $\boldsymbol{f}_j^k$ and Δ_{jt}^k would constitute the generalized force distribution and the target interstory demand pair for the k'th frame in the system. This, however, creates a significant amount of workload. The procedure can be simplified by applying the GPA force vectors at the centers of mass (Eq. 16) rather than at each frame individually, while tracking the target interstory drifts of each frame separately (Eq. 26). Along a story, different frames reach their target interstory drifts at different analysis steps. However, the member responses obtained at these steps are virtually the same as the ones that are achieved when performing a full, frame by frame analysis. Application of generalized force vectors defined at the center of mass significantly reduces the computational effort. To illustrate on the 8-story, 4-frame structure, only 8 pushover analyses are performed and 32 target interstory drift ratios are searched from the frame interstory drifts. Due to the simplicity offered by this approach and the ability to produce results with similar accuracy compared to frame-by-frame analysis, the GPA procedure is implemented in this simplified form.

4. Generalized Pushover Analysis Algorithm

1. *Eigenvalue analysis*: Periods (T_n), mode shapes ($\boldsymbol{\varphi}_n$) and associated modal properties of the structure are determined.
2. *Response spectrum analysis*: Spectral accelerations (A_n) and displacements (D_n) of each mode are determined from the corresponding linear elastic response spectrum. Then, $\Delta_{j,n}$ and $\Delta_{j,max}$ for the center of mass are obtained from Eq. (9), and $\Delta_{j,n}^k$ and $\Delta_{j,max}^k$ for each frame k are obtained from Eq. (20) by using these spectral quantities.
3. *GPA force vectors*: GPA force vectors $\boldsymbol{f}_j$ are determined according to Eq. (16).
4. *Target interstory drift demands*: Frame target interstory drift demands (Δ_{jt}^k) are also determined by using Eq. (26).
5. *Nonlinear static analysis*: $\boldsymbol{f}_j$ are acted upon the system in an incremental form until Δ_{jt} calculated in step 4 is exceeded. Then the interstory drift record of frame k is searched for Δ_{jt}^k. The analysis step that yields Δ_{jt}^k is used to compile the member deformations and internal forces at the j'th story of frame k (target analysis step). Nonlinear static analysis is repeated for each story, j = 1 to N.
6. *Determination of structural responses*: Using the target analysis steps obtained in the 5th step, deformations and internal forces of all members at each frame are determined directly from the deformation state of the structure at the target interstory drift demand. Entire response of the system is then compiled by employing an envelope algorithm where absolute maxima of these internal forces and deformations are selected for every structural member without using any modal combination rule. These results are registered as final response estimates.

GPA procedure is implemented to an eight story torsionally coupled frame building under fifteen ground motions in the case study presented below.

4. Eight Story Frame Building

The story plan of the eight story moment resisting frame building is shown in Fig 2. The building is designed in compliance with the Turkish Earthquake Code [16] by employing the capacity design principles, with an enhanced ductility level (R=8). The design spectrum for soft soil conditions is shown in Fig 3. Concrete and steel characteristic strengths are 25 MPa and 420 MPa, respectively. Uniform member dimensions are selected in the design of beams and columns. Beams are 30x55 cm and columns are 50x50 cm throughout the building. Slab thickness at all floors is 14 cm and live load is 2 kN/m^2. Ground story height is 3.5 meters whereas the height of other stories is 3 meters. Asymmetry and the resulting torsional coupling are provided by offsetting the mass center of the building from the center of stiffness by 15% of the plan dimension. Thus, asymmetric mass distribution is obtained along the direction of analysis (Y-axis in Fig. 2). Frames of the structure in the direction of analysis are named according to their expected deformation patterns.

The structure is modeled by using the OpenSees software [17]. A linear elastic model is developed for performing linear elastic response spectrum analysis, and a nonlinear structural model is prepared in order to perform nonlinear response history analysis, generalized pushover analysis and conventional (single mode) pushover analysis. Linear elastic model is composed of "ElasticBeamColumn" elements where the gross moments of inertia of the beams and columns are multiplied by 0.4 and 0.6 respectively, in order to account for the cracked section stiffnesses of reinforced concrete members. "BeamwithHinges" element is employed in the nonlinear structural model both for beams and columns. Plasticity is lumped along the plastic hinge length which is half of the section depth at all members. Moment-curvature relationships are assigned to the beam ends with elasto-plastic hysteresis relations whereas fiber sections are selected in order to introduce plasticity in the column ends. P-Delta effects are considered in the analytical models. Rayleigh damping is used in both models where the damping coefficients are obtained from the 1'st and 3'rd modes that are assigned 5% viscous damping.

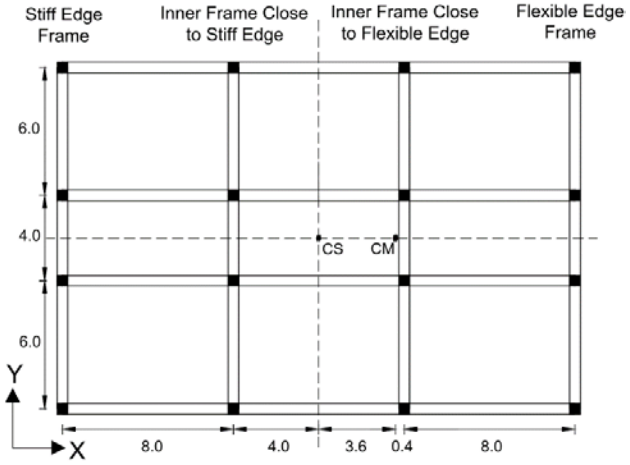

Fig. 2 Plan view of the eight-story unsymmetrical-plan structure (all units in meters).

Free vibration periods of the first four coupled modes are 1.62, 1.03, 0.52 and 0.33 seconds. The first and third modes are translation dominant whereas the second and fourth modes are rotation dominant. Hence, the structure is torsionally stiff. Translational modes in the x-direction are not considered.

Fifteen ground motion records have been randomly selected from the PEER Strong Motion Database [18] and used without employing a scaling or any other modification to the original data. These ground motions produce different levels of inelastic deformation demands and higher mode effects (both in elevation and plan) in the frame structure. Their acceleration spectra and record properties are given in Fig. 3 and Table 1, respectively.

The linear elastic design spectrum (unreduced) and the mean spectrum of fifteen ground motions are also shown in Fig. 3. The selected ground motions do not represent any commonality or membership to a family.

Table 1. Strong ground motions and their properties

GM No.	NGA Code	Earthquake	Mw	PGA (g)	Site Geology
GM1	H-E04140	Imperial Valley - 1979	6,5	0,485	D
GM2	ERZ-EW	Erzincan - 1992	6,9	0,496	D
GM3	CLS090	Loma Prieta - 1989	7,0	0,479	A
GM4	SPV270	Northridge - 1994	6,7	0,753	D
GM5	PCD254	San Fernando - 1971	6,6	1,160	B
GM6	BOL000	Duzce - 1999	7,1	0,728	D
GM7	ORR090	Northridge - 1994	6,7	0,568	B
GM8	ORR360	Northridge - 1994	6,7	0,514	B
GM9	B-PTS315	Superstition Hills - 1987	6,6	0,377	D
GM10	IZT090	Kocaeli - 1999	7,4	0,220	A
GM11	DZC270	Kocaeli - 1999	7,4	0,358	D
GM12	LCN275	Landers - 1992	7,3	0,721	A
GM13	G066090	Morgan Hill - 1984	6,1	0,292	A
GM14	NPS210	N. Palm Springs - 1986	6,2	0,594	D
GM15	STG000	Loma Prieta - 1989	7,0	0,513	D

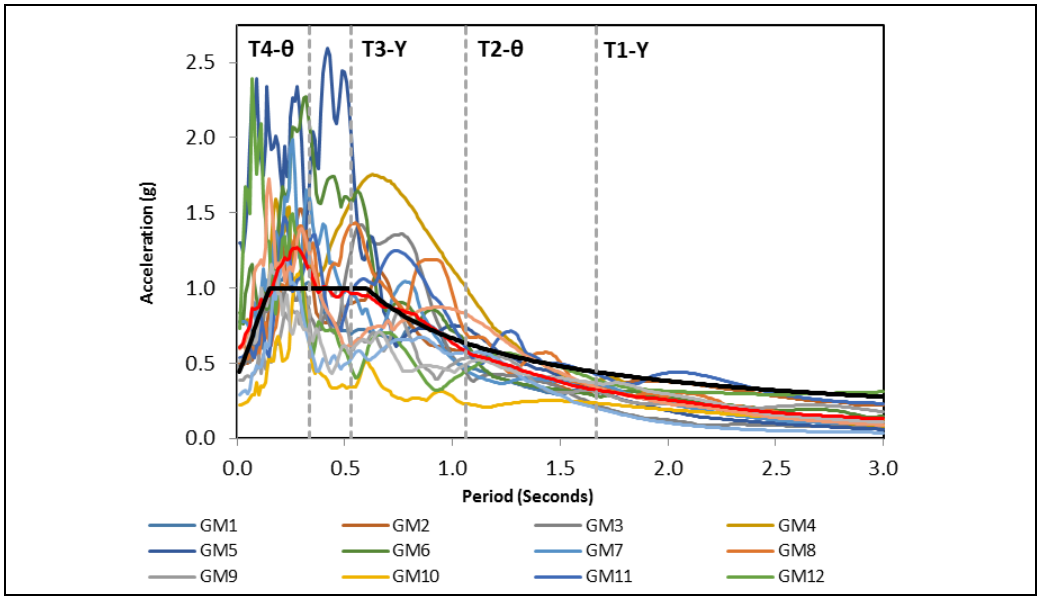

Fig. 3 Acceleration response spectra of the fifteen ground motions and the design spectrum (T1-Y, T2-θ, T3-Y, T4-θ indicate the first four modal periods and the dominant response directions)

Two different types of results are presented in the following paragraphs. The first type includes response results to three individual ground motions selected from Table 1. These ground motions produce different levels of inelastic deformations, from lower to higher. The second type of results includes statistical evaluation of the responses to the total set of fifteen ground motions. All results in the two categories are assessed with reference to the results of benchmark nonlinear response history analysis (NRHA).

For purposes of brevity, two sets of response results of varying intensity are presented for each selected ground motion in Figs. 4-5. These are the height-wise variations of interstory drift ratio, mean beam-end plastic rotations and story shears given for each frame separately. The results of GPA are compared with the results of benchmark NRHA in all figure boxes.

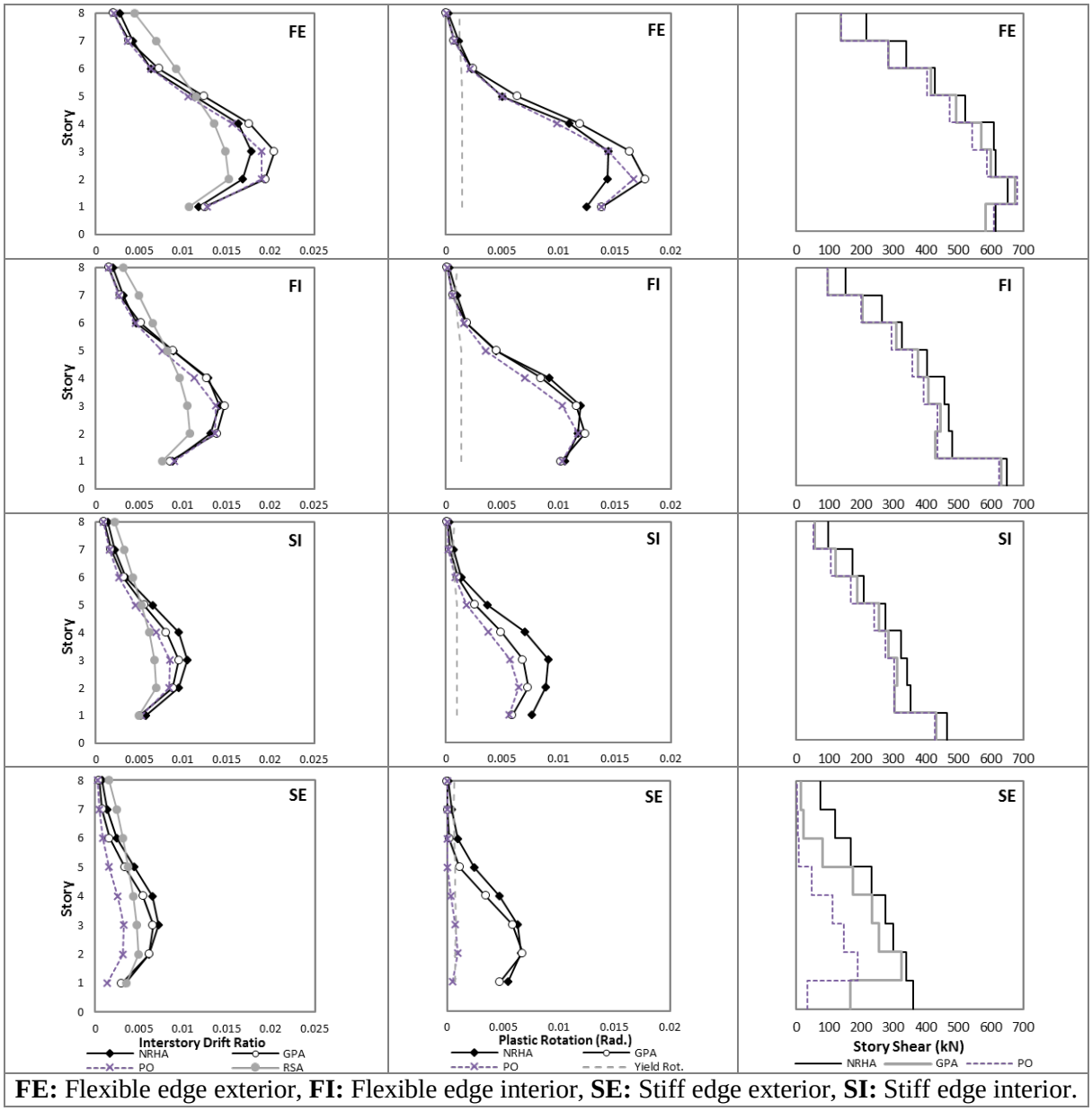

FE: Flexible edge exterior, **FI:** Flexible edge interior, **SE:** Stiff edge exterior, **SI:** Stiff edge interior.

Fig. 4 The distribution of interstory drift ratios, mean beam-end plastic rotations and story shears in each frame under the IZT090 ground motion.

The results of conventional (single mode) pushover analysis (PO) are also provided in each figure for observing the contribution of higher modes. First mode load pattern in PO includes torsional moments and first mode inelastic response is employed in calculating the target roof displacement. Moreover, interstory drift ratios obtained by the linear elastic response spectrum analysis (RSA) are presented along with the results of nonlinear procedures in order to assess the validity of linear elastic models with cracked section properties in predicting the interstory drift distributions in a torsionally coupled system which undergoes different levels of inelastic deformations.

The results obtained under the IZT090 ground excitation are shown in Fig. 4. This is the weakest intensity ground motion in Table 1; however, it produces interstory drift ratios of 1.8% and mean beam plastic rotations of 0.014 radians at the middle stories of the flexible edge exterior (FE) frame, as calculated by NRHA. GPA predicts the interstory drifts and beam plastic rotations quite well, and story shears perfectly in all frames. The improvement of GPA over PO is also notable in all frames, particularly at the stiff edge frame (SE) for all three response parameters. Interstory drift distributions predicted by RSA are fairly acceptable for this ground motion

since the inelastic deformations are not so far into the plastic range as observed in the second column boxes of Fig. 4. Negligible yielding of columns occurs at the base sections, with maximum plastic rotations not exceeding 0.1%.

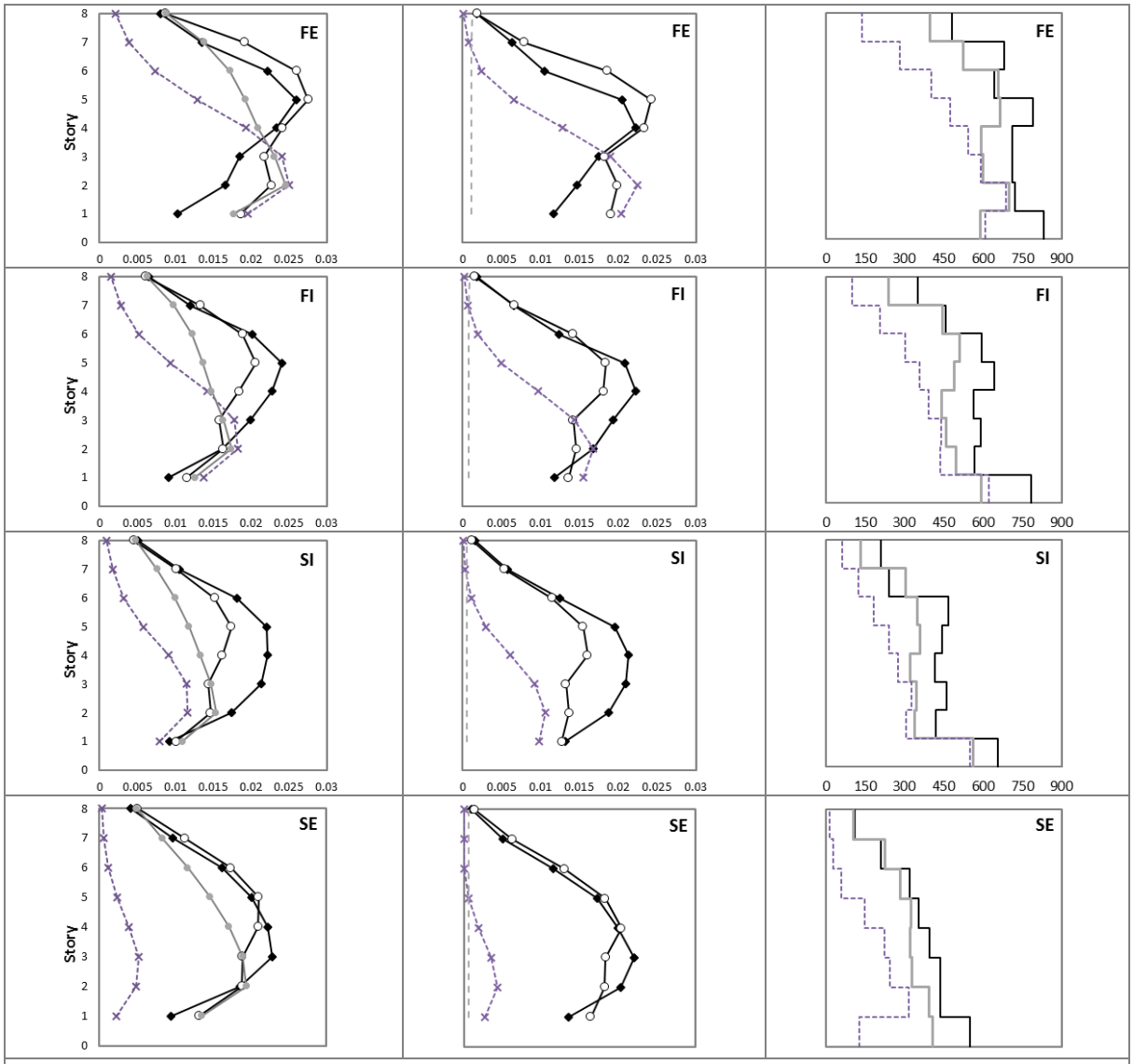

FE: Flexible edge exterior, **FI:** Flexible edge interior, **SE:** Stiff edge exterior, **SI:** Stiff edge interior.

Fig. 5 The distribution of interstory drift ratios, mean beam-end plastic rotations and story shears in each frame under the SPV270 ground motion.

A significant higher mode response is observed in Fig. 5 under SPV270, accompanied with large inelastic deformations. Maximum values of interstory drift ratios and mean beam plastic rotations calculated by NRHA are 2.6% and 0.022 radians, respectively. GPA generally predicts both the interstory drifts, mean beam plastic deformations and story shears of all frames successfully, with an under-estimation of deformations by about 30% at the middle stories of the SI frame. RSA analysis gives reasonable interstory drifts at the lowest three stories, but completely misses the upper stories where higher modes contribute significantly. This is a result of the quadratic combination of linear elastic modes which is usually a poor assumption when the first mode is not dominant. Mean rotation ductilities of the beam ends are in the 10-25 range in the 1st story, in the 15-40 range in the 3rd story (maximum), and around 3 in the top story under SPV270. Maximum rotation ductility demand at the base of the first story column of the flexible edge frame is 1.7.

The second type of results provide comparisons of the statistical distributions of interstory drift ratios, beam plastic rotations and story shears under fifteen ground motions. The statistical distribution of interstory drift ratios calculated by NRHA and GPA at the four frames is shown in the left-hand side four-plot set of Fig. 7. It can be observed that the distributions obtained at the FI and SE frames are matching perfectly well whereas those obtained at the FE and SI frames are in reasonably good agreement. Moreover, mean interstory drift distributions are also calculated under the mean spectrum of fifteen ground motions shown in Fig. 3. These results are fairly close to the mean of fifteen interstory drift distributions obtained under fifteen ground motions separately. Therefore, it can be concluded that GPA conducted under a mean spectrum of ground motions produces acceptable estimates of the statistical mean of interstory drift ratios obtained under a set of ground motions. Accordingly, GPA can be employed as an effective nonlinear analysis tool under a site specific design spectrum representing the mean spectrum of ground motions expected at a site.

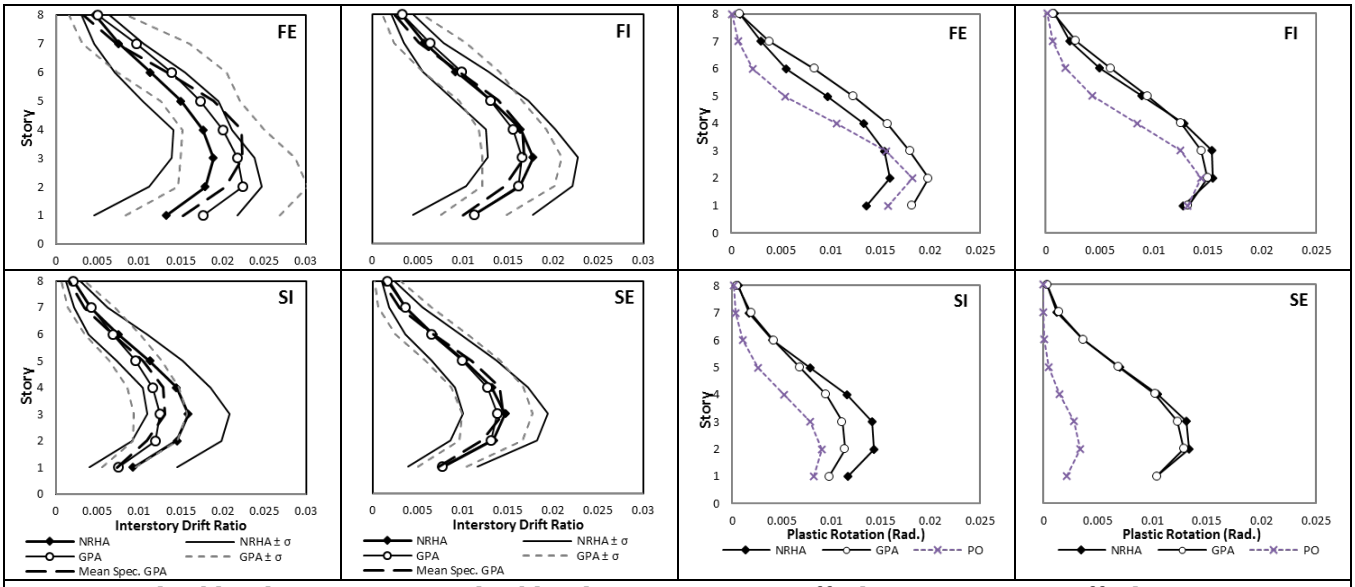

FE: Flexible edge exterior, **FI:** Flexible edge interior, **SE:** Stiff edge exterior, **SI:** Stiff edge interior.

Fig. 7 The distribution of interstory drift ratios and mean spectrum GPA results and distribution of mean beam-end plastic rotations in each frame.

The mean distribution of beam plastic rotations obtained under fifteen ground motions calculated by NRHA, GPA and PO are compared in right-hand side of Fig. 7. It has to be reminded that beam plastic rotations are also the mean values over the beam ends in each story. The results in Fig. 7 reveals that mean GPA and mean NRHA results match perfectly well in the FI and SE frames, and match reasonably well in the FE and SI frames.

4. SUMMARY AND CONCLUSIONS

Generalized pushover analysis procedure is extended to 3D torsionally coupled systems in this study. Modal contributions to the generalized force vectors and target interstory drifts are calculated by a modal scaling rule which is based on the complete quadratic combination. Generalized forces are applied to the mass centers of each story incrementally for producing nonlinear static response. Maximum response quantities are obtained at the loading increments when the individual frames attain their own target interstory drift values in each story. GPA requires (N) pushovers in each direction where N is the number of stories.

GPA is non-adaptive; hence it can be implemented conveniently with any general purpose nonlinear static analysis tool. Also it does not suffer from the statistical combination of inelastic modal responses which leads to violation of force equilibrium. Convergence is the basic advantage of GPA as well as all nonlinear static procedures over the nonlinear response history analysis procedure. NRHA suffers from convergence problems when the size of the model is large as in a 3D structure, when the model involves computationally demanding elements such as fiber elements, and when the ground motions drive the system far into significant inelastic deformation range.

GPA predicts the results of NRHA fairly well, as demonstrated under several ground motions employed in this study. Moreover, GPA conducted under the mean spectrum of a set of ground motions produce results which are very close to the mean of individual GPA results. This is an indication that GPA can be employed as an effective nonlinear analysis tool under a site specific design spectrum.

The basic limitation of the GPA procedure arises from the local accumulation of plastic deformations during actual dynamic response, which leads to significant changes in the modal deformation shapes. The non-adaptive GPA algorithm cannot track these changes and hence its results may deviate from the results of NRHA when such localized nonlinearities dominate the overall deformation pattern of the system.

5. References

[1] Rutenberg A, Heidebrecht A.C. (1975), "Approximate Analysis of Asymmetric Wall-frame Structures", *Building Science*, **10**(1): 27–35.

[2] Reinhorn A, Rutenberg A, Glück J. (1977) "Dynamic Torsional Coupling in Asymmetric Building Structures", *Building and Environment*, **12**(4): 251–261.

[3] Rutenberg A. (1998), "EAEE Task Group 8. Behavior of Irregular and Complex Structures, State of the Art Report: Seismic Nonlinear Response of Code-Designed Asymmetric Structures", *Proceedings of the 11th European Conference on Earthquake Engineering*, Paris.

[4] Kosmopoulos A, Fardis M.N. (2006), "Seismic Evaluation of Strongly Irregular and Torsionally Unbalanced Concrete Buildings", *Proceedings of the 2nd FIB Congress*, Naples.

[5] Comité European de Normalisation, (2005), "Eurocode 8, Design of Structures for Earthquake Resistance - Part 3: Assessment and Retrofitting of Buildings", *European Standard EN 1998-3*, Brussels.

[6] Kilar V, Fajfar P. (1997), "Simple Push-Over Analysis of Asymmetric Buildings", *Earthquake Engineering and Structural Dynamics*, **26**(2): 233–249.

[7] Moghadam AS, Tso W.K. (1998), "Pushover Analysis for Asymmetrical Multistory Buildings", *Proceedings of the 6th U.S. National Conference on Earthquake Engineering, EERI*, Oakland, California.

[8] Chopra AK, Goel R.K. (2004), "A Modal Pushover Analysis Procedure to Estimate Seismic Demands for Unsymmetric-plan Buildings", *Earthquake Engineering and Structural Dynamics*, **33**(8): 903–927.

[9] Chopra AK, Goel R.K. (2002), "A Modal Pushover Analysis Procedure for Estimating Seismic Demands for Buildings", *Earthquake Engineering and Structural Dynamics*, **31**(3): 561–582.

[10] Fajfar P, Marusic D, Perus I. (2005), "Torsional Effects in the Pushover-Based Seismic Analysis of Buildings", *Journal of Earthquake Engineering*, **9**(6): 851–854.

[11] Fajfar P. (2000), "A Nonlinear Analysis Method for Performance-Based Seismic Design", *Earthquake Spectra*, **16**(3): 573–592.

[12] Kreslin M, Fajfar P. (2012), "The Extended N2 Method Considering Higher Mode Effects in Both Plan and Elevation", *Bulletin of Earthquake Engineering*, **10**: 695–715.

[13] Barros RC, Almeida R. (2011), "Pushover Analysis of Asymmetric Three-Dimensional Building Frames", *Journal of Civil Engineering and Management*, **11**(1): 3–12.

[14] Sucuoğlu H, Günay M.S. (2011), "Generalized Force Vectors for Multi-mode Pushover Analysis", *Earthquake Engineering and Structural Dynamics*, **40**(1): 55–74.

[15] Wilson EL, Der Kiureghan A, Bayo E.P. (1981), "A Replacement for the SRSS Method in Seismic Analysis", *Earthquake Engineering and Structural Dynamics*, **9**(2): 187–192.

[16] Turkish Ministry of Construction and Settlement. (2007), "Design Code for Buildings in Seismic Regions", Ankara.

[17] Open System for Earthquake Engineering Simulation, (2015), Available from: http://opensees.berkeley.edu.

[18] PEER Strong Motion Database, (2015), Available from: http://ngawest2.berkeley.edu